


The infrared traced star formation rates of associated absorption lines quasars

ZHE-GENG CHEN,^{1,2} RUI-JING LU ,¹ ZHI-FU CHEN,² WEN-QIANG LIANG,¹ XING-LONG PENG,² JING LI,¹ AND WEI-RONG HUANG²

¹*Guangxi Key Laboratory for Relativistic Astrophysics, School of Physical Science and Technology, Guangxi University, Nanning 530004, People's Republic of China*

²*School of Physics and Electronic Information, Guangxi Minzu University, Nanning 530006, People's Republic of China*

Accepted to ApJ

ABSTRACT

Some optically selected quasars exhibit Mg II associated absorption lines (AALs), and its origin remains unclear. In this paper, we compile a sample of 1769 quasars, with or without Mg II AALs. Of which 1689 are Far-Infrared (FIR) detected quasars and the rest are not detected in FIR. For the FIR undetected quasars, we obtain stacks for both with and without Mg II AAL quasars. Then we estimate the star formation rates (SFRs) within quasar host galaxies based on their FIR luminosities derived from their FIR greybody components, and find that, although quasars with Mg II AALs have significantly redder median composite spectra than those without Mg II AALs, the SFR distributions of the two types of quasars are statistically indistinguishable. These results do not require an evolutionary link between the quasars with and without Mg II AALs, and would be reconciled if an orientation effect cannot be ignored among the quasars hosting different types of absorption lines.

Keywords: galaxies: general — galaxies: active — quasars: absorption lines

1. INTRODUCTION

The star formation rate (SFR) is a crucial astrophysical tracer for understanding the formation and evolution of galaxies (Zhuang & Ho 2019). In the evolutionary process of galaxies, active galactic nucleus (AGNs) could be triggered by gas-rich galaxy mergers, leading to black hole accretion and bursts of star formation in host galaxies (Sanders et al. 1988; Hopkins et al. 2008, 2016). A substantial amount of gas and dust is required to funnel inward to fuel black hole accretion and star-forming activities, which also contributes to the obscuration of young AGNs. As the central black hole grows, the jet and wind, which originate in the central regions of AGNs, subsequently generate feedback to surrounding environments, potentially enhancing or quenching the star formation rate (SFR) within host galaxies (e.g., Fabian 2012; Gaibler et al. 2012; Bieri et al. 2016; Chen et al. 2022).

The gas clouds that are far beyond the gravitational bound of quasar systems often produce absorption lines with redshifts much less than those of quasar systems ($z_{abs} \ll z_{em}$) in quasar spectra, which are generally called intervening absorption lines and often host line widths less than a few hundred km s^{-1} (narrow absorption lines, NALs). Whilst, the gas medium within the gravitational bound of quasar systems often produces absorption lines with $z_{abs} \approx z_{em}$, which are often called as associated absorption lines (AALs) and have a wide range of line widths. Thus the AALs can be further divided into three subclasses based on their line widths: (1) broad absorption lines (BALs) with line widths generally larger than 2000 km s^{-1} ; (2) NALs; and (3) Mini-BALs with line widths between the BALs and NALs. Meanwhile, according to the ionization levels of transition lines, the AALs can be categorized into high-ionization AALs (HiAALs, e.g., Si IV $\lambda\lambda 1393, 1402$; C IV $\lambda\lambda 1548, 1551$) and low-ionization AALs (LoAALs, e.g., Mg II $\lambda\lambda 2796, 2803$; Al III $\lambda 1854$).

About 30% of optically selected quasars exhibit AALs (e.g., Gibson et al. 2009; Allen et al. 2011; Chen et al. 2016, 2018; Peng et al. 2024). Therefore, AALs serve as

a useful tool to probe the physical environments within quasar systems.

Some studies have shown that quasars with LoAALs (including LoBALs, LoMini-BALs, and LoNALs) have significantly higher SFR than those without AALs (Non-AALs) (e.g., [Chen et al. 2022](#); [Peng et al. 2024](#)).

Whereas, different results have also been reported that quasars with high-ionization broad absorption lines (HiBALs) exhibit a SFR consistent with those without BALs (Non-BALs) (e.g., [Willott et al. 2004](#); [Cao Orjales et al. 2012](#); [Pitchford et al. 2016](#)).

There are main two schemes for explaining whether the quasars host AALs: the orientation-dependent and evolution schemes. In the evolution scheme, the quasars hosting AALs are often considered to live in the gas-rich environment of the early stages of galaxy evolution (e.g., [Boroson 1992](#); [Wang et al. 2016](#); [Bouché et al. 2016](#); [Chen et al. 2022](#)). Consequently, the AAL quasar often host intense star formation activity and thus has high dust masses which will yield higher FIR emission. When the quasar evolves from the AALs to the Non-AALs, the SFRs within host galaxies naturally reduce if the powerful outflows of quasars sweep out the interstellar gas. In the orientation-dependent hypothesis (e.g., [Antonucci 1993](#); [Urry & Padovani 1995](#); [Hamann et al. 2012](#)), AALs are likely to appear in spectra if the quasar’s line of sight is close to the accretion disk, otherwise they are unlikely to appear. Consequently, the SFR within the host galaxy does not depend on whether the quasar has AALs.

The UV-optical tracers of the SFR, such as [O II], H α emission lines (e.g., [Shen & Ménard 2012](#); [Madau & Dickinson 2014](#); [Chen et al. 2020](#); [Peng et al. 2024](#)), are susceptible to the dust attenuation and the contamination from quasar central regions (e.g., [Kennicutt 1998](#); [Calzetti et al. 2000](#); [Khostovan et al. 2020](#)). To better assess the SFR within the host galaxy, many previous efforts have mainly focused on corrections for both the dust attenuation and the contamination from quasar emissions (e.g., [Zhuang & Ho 2019](#)). However, these corrections may also invoke other biases. The dust attenuation at FIR wavelength is generally considered as negligible. Consequently, the FIR emission is an important tracer of the SFR within host galaxy. Using the FIR tracer of the SFR, [Cao Orjales et al. \(2012\)](#) claimed that the HiBAL quasars exhibit the similar SFRs with the Non-BAL ones, which may be partly due to the fact that the HiBAL quasars are at an evolutionary stage close to the Non-BAL quasars. The evolutionary stage of the LoAAL quasars, including LoBALs, LoMini-BALs, and LoNALs, is likely far away from that of the Non-AAL quasars (e.g., [Chen et al. 2022](#); [Peng et al. 2024](#)). There-

fore, we compile a sample of quasars with FIR observations to compare the SFR within host galaxies between the LoAAL and Non-LoAAL quasars.

Throughout this work, we assume a flat Λ CDM cosmology with $\Omega_m = 0.3$, $\Omega_\Lambda = 0.7$, and $h_0 = 0.7$.

2. DATA AND ANALYSIS

2.1. Quasar sample

The Sloan Digital Sky Survey (SDSS; [York et al. 2000](#)) collected quasar spectra at a resolution $R \approx 2000$ in wavelength ranges of $\lambda \approx 3800 - 9200 \text{ \AA}$ (SDSS-I/II [Abazajian et al. 2009](#)), or $\lambda \approx 3600 - 10500 \text{ \AA}$ (SDSS-III/IV [Smee et al. 2013](#); [Dawson et al. 2013](#)). The Sixteenth Data Release (DR16Q) is the final dataset for the SDSS-IV quasar catalog ([Lyke et al. 2020](#)), which contains 750,414 quasars. In this work, we aim to study quasars with and without Mg II $\lambda\lambda 2796, 2803$ AALs. Therefore, to ensure reliable detection of Mg II $\lambda\lambda 2796, 2803$ absorption lines in the SDSS spectra, if any, we select the quasars with $0.3 < z_{\text{em}} < 2.0$ from the SDSS DR16Q.

To obtain the integrated FIR luminosities from the spectral energy distributions (SED) of quasars, we collect their corresponding photometric data at mid-infrared (MIR) 3.4 μm (W1), 4.6 μm (W2), 12 μm (W3), and 22 μm (W4) from the data catalog of the Wide-field Infrared Survey Explorer (WISE; [Assef et al. 2018](#)), and at FIR 250 μm , 350 μm , and 500 μm from the *Herschel* catalog ([Viero et al. 2014](#); [NHSC 2020a,b,c](#)). Due to the fact that most of the SDSS quasars are not detected in the W4 band (e.g., [Bianchini et al. 2019](#); [Lyke et al. 2020](#)), and given that during the WISE mission, the W4 band became unusable due to the depletion of its solid hydrogen cryogen, the W1, W2, and W3 bands continued with another half-sky scan. Thus, the data from the W4 band are excluded from our analysis. We initially arrive at a total of 1779 quasars, all having the 3.4 μm , 4.6 μm , 12 μm , 250 μm , 350 μm , and 500 μm photometric data. 90 of 1779 quasars have flux densities under the nominal 3σ depths of 17.4, 18.9, and 20.4 mJy at 250, 350, and 500 μm , respectively ([Nguyen et al. 2010](#); [Netzer et al. 2016](#)), which are classified into FIR undetected quasars. Among the FIR undetected quasars, 10 are excluded because they are located too close to the edge of their respective fields for further stacking analysis. We finally arrive at a total of 1769 quasars. Of these, 1689 are FIR detected quasars, and 80 are FIR undetected ones.

Based on the SDSS DR16Q catalog, previous works ([Chen et al. 2018, 2022](#); [Peng et al. 2024](#)) have systematically searched for the Mg II AALs within the velocity

offset $|v_{\text{off}}|^1$ of 3000 km s^{-1} around Mg II emission lines. Following the same method, in order to work on a well-defined, high-quality sample of quasars with and without Mg II AALs, in this paper, we construct a sample of quasars with Mg II AALs within $|v_{\text{off}}| < 1500 \text{ km s}^{-1}$ (Mg II AAL quasars hereafter), and sample of quasars without Mg II AALs $|v_{\text{off}}| < 6000 \text{ km s}^{-1}$ (Non-Mg II AAL quasars hereafter). Of the 1769 quasars, 189 have Mg II AALs, and 1580 do not. Of the 189 AAL quasars, 182 have the FIR detections and 7 do not. While, Of the 1580 Non-AAL quasars, 1507 have the FIR detections, and 73 do not. As shown in Figure 1, the two types of quasars share almost the same redshift distribution with a median redshift of 1.35.

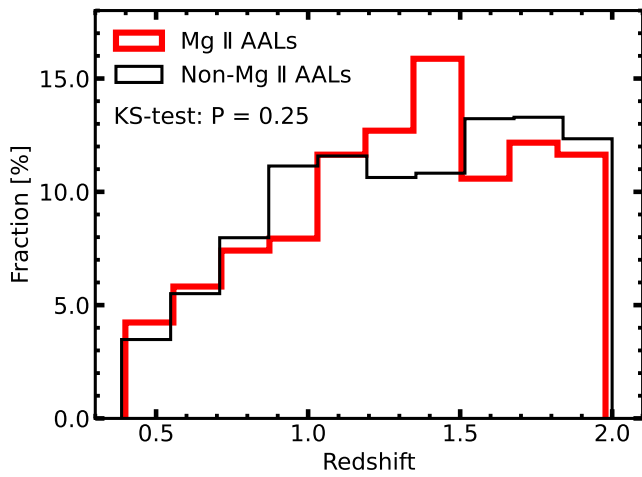


Figure 1: Redshift distributions for the quasars with and without Mg II AALs. The KS test yields a probability $p = 0.25$.

2.2. SED fitting and FIR SFR

The IR emission of galaxies comes mainly from the combined contribution of older stellar populations, AGNs, and star formation (SF) (e.g., Madau & Dickinson 2014; Galliano et al. 2008; Ciesla et al. 2015), in which, the AGN contribution is primarily originated in the dusty environment (the dust in the torus and clouds), which drops sharply at longer wavelengths, and negligible at $\lambda \gtrsim 30 \mu\text{m}$ (e.g., Mor & Netzer 2012; Symeonidis et al. 2016; Lani et al. 2017). Meanwhile, the older stellar population contribution is dominated by the radiations at $\lambda \lesssim 2 \mu\text{m}$. Thus, this contribution to the FIR luminosity is also negligible (e.g., Pitchford

et al. 2016; Wethers et al. 2020). The SF contribution to IR emission mainly originates from the re-radiation of dust, which absorbed the UV emission primarily from star formation. This contribution is characterized by a greybody model (Casey 2012):

$$S(\lambda, T) \propto (1 - e^{-[\frac{\lambda_0}{\lambda}]^\beta}) \frac{1}{\lambda^5} \frac{1}{e^{hc/\lambda kT} - 1}, \quad (1)$$

where λ_0 represents the wavelength at which optical depth reaches unity (Draine 2006), T is the dust temperature constrained within 15–60 K (e.g., Madau & Dickinson 2014; Wethers et al. 2020), spanning the full range of observed dust temperatures for quasar hosts of our sample, and β is the emissivity index with a fixed value of $\beta=1.6$ (Priddey & McMahon 2001).

As analyzed above, the IR emission of quasars could simultaneously fit a total model with a combination of the two components, i.e.

$$M_{\text{tot}} = X_{\text{torus}} \times M_{\text{torus}}(\lambda) + X_{\text{SF}} \times S(\lambda), \quad (2)$$

where the M_{torus} represents the AGN contribution, which was derived from 115 type-I AGNs (Lani et al. 2017), and the two components of M_{torus} and $S(\lambda)$ are scaled by the factors of X_{torus} and X_{SF} , respectively. Throughout the fitting, we take the two vertical scalings and the dust temperature of the greybody template as free parameters, with 6 data points for each of quasars in our sample. In order to obtain full posterior distributions on the best-fitting model parameters and to marginalize over any nuisance parameters, we utilize Bayesian approach and Markov chain Monte Carlo (MCMC) sampling based on the Python package `emcee` (Foreman-Mackey et al. 2013), and finally get the best dust temperature T , X_{torus} and X_{SF} , respectively. As an example, Figure 2 shows the best fit model to the observation of quasar J094729.14 + 381033.2. With the best fitting parameters, we obtain the FIR luminosity (L_{FIR}) of quasar by integrating the greybody curve (see the red-dotted line of Figure 2) from 8 to $1000 \mu\text{m}$. Thus the SFR within its host galaxy can be estimated with the original empirical relation derived by Kennicutt (1998):

$$\text{SFR}(M_\odot \text{ yr}^{-1}) = 4.5 \times 10^{-44} L_{\text{FIR}} (\text{erg s}^{-1}), \quad (3)$$

that assumes a continuous starbursts of age 10 — 100 Myr. For the FIR detected quasars included in our final sample, the resulting SFR are listed in Table 1.

2.3. Stacks of the FIR undetected quasars

Stacking FIR images based on optically measured positions of FIR undetected quasars could reduce confusion, thereby enhances the accuracy of the mean flux

¹ $v_{\text{off}} = \frac{(1+z_{\text{abs}})^2 - (1+z_{\text{em}})^2}{(1+z_{\text{abs}})^2 + (1+z_{\text{em}})^2}$

Table 1: The properties of the sample

SDSS name	PLATE	MJD	FIBERID	z	$S_{3.4}$ mJy	$S_{4.6}$ mJy	$S_{12.0}$ mJy	S_{250} mJy	S_{350} mJy	S_{500} mJy	$\log M_{\text{BH}}$ M_{\odot}	SFR $M_{\odot} \text{ yr}^{-1}$	AAL	FIR detected?
000022.44-031041.5	7895	57659	918	1.2011	0.031 ± 0.005	0.065 ± 0.011	0.049 ± 0.129	64.0 ± 19.7	79.2 ± 18.0	73.0 ± 17.9	8.45	330^{+68}_{-49}	0	yes
000055.41-012006.0	7850	56956	734	1.7581	0.034 ± 0.005	0.050 ± 0.010	0.151 ± 0.111	32.0 ± 6.2	38.2 ± 6.8	24.2 ± 6.6	8.67	397^{+80}_{-51}	0	yes
000059.09-013722.6	7850	56956	280	1.6835	0.066 ± 0.005	0.083 ± 0.010	0.020 ± 0.125	50.2 ± 8.3	43.9 ± 10.2	33.2 ± 7.9	8.84	550^{+130}_{-84}	0	yes
000100.36-021237.3	7850	56956	266	1.2979	0.033 ± 0.005	0.089 ± 0.011	0.036 ± 0.134	82.7 ± 15.8	82.7 ± 20.8	67.1 ± 20.7	8.53	473^{+96}_{-73}	0	yes
000122.41-000130.6	7848	56959	18	1.4830	0.150 ± 0.005	0.238 ± 0.010	0.178 ± 0.110	91.0 ± 13.9	92.7 ± 16.8	59.0 ± 16.9	8.01	733^{+165}_{-89}	1	yes

Note — Numbers of “0” and “1” in column ‘AAL’ represent the spectra without or with Mg II AALs.
(This table is available in its entirety in machine-readable form.)

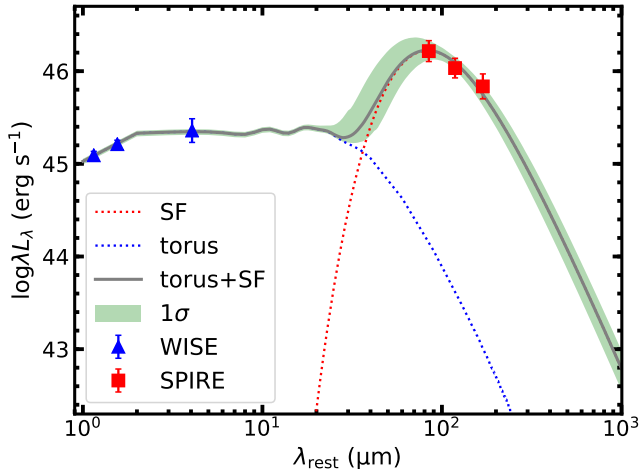


Figure 2: The best SED fit to the quasar *J094729.14+381033.2*. Blue squares represent the WISE photometries at 3.4 μm , 4.6 μm , and 12 μm . Red squares represent the *Herschel* photometries at 250 μm , 350 μm , and 500 μm . The blue-dotted line represents the contribution from the AGN (Lani et al. 2017), the red-dotted line represents the contribution from the greybody emission (Casey 2012), and grey-solid line is the sum of the blue-dotted and red-dotted lines. Green-shaded region marks 68% credible interval of the best model.

density measurements (e.g., Crichton et al. 2016; Stanley et al. 2017; Bianchini et al. 2019). To yield the mean flux densities at 250 μm , 350 μm , and 500 μm for the FIR undetected quasars, we here stack the FIR images observed by *Herschel* based on the optically measured positions (e.g., Valiante et al. 2016). We briefly describe the main processes as follows. We cut the image around each FIR undetected quasar with a set size of $5' \times 5'$, and stack the cutting images using the inverse of the noise as the weight. A combination of a 2D Gaussian plus a constant background is invoked to fit the stacked image. The resulting peak value is taken as the mean flux density. The corresponding uncertainty is yielded with the bootstrap technique. Using the same method shown in Section 2.2,

we also estimate their SFRs and yield $73^{+41}_{-25} M_{\odot} \text{ yr}^{-1}$ and $65^{+16}_{-13} M_{\odot} \text{ yr}^{-1}$ for the quasars with and without Mg II AALs, respectively, which indicates that there is no statistically significant difference in SFRs of the two types of FIR undetected quasars.

3. DISCUSSIONS AND CONCLUSIONS

We have compiled a sample of 1769 quasars with $0.3 < z_{\text{em}} < 2.0$ from the SDSS DR16Q, among which 189 quasars are detected Mg II AALs within $|v_{\text{off}}| < 1500 \text{ km s}^{-1}$, and 1580 quasars are without detected Mg II AALs within the spectral data within $|v_r| < 6000 \text{ km s}^{-1}$. All of these 1769 quasars have been observed by the WISE at 3.4 μm , 4.6 μm , 12 μm , and by the *Herschel* at 250 μm , 350 μm , and 500 μm . Among the 189 quasars with Mg II AALs, *Herschel* FIR flux densities of 7 quasars are below the 3σ threshold, which are classified as FIR undetected quasars. Among the 1580 quasars without Mg II AALs, 73 quasars are below the 3σ threshold, which are also classified as FIR undetected quasars.

We employ a model with a combination of two components (AGN torus+ star-forming galaxy) to fit the combined photometrical data (WISE + SPIRE) of each FIR detected quasar in our sample, and estimate their SFRs based on their integrated luminosities at FIR. Figure 3 shows the distributions of the SFRs for the FIR detected quasars with (red line) and without (black line) Mg II AALs, with the medians of 335^{+505}_{-215} and $320^{+465}_{-219} M_{\odot} \text{ yr}^{-1}$ for the quasars with and without Mg II AALs, respectively. A two-sided KS-test on the two distributions finds no statistically significant difference between them with a null probability of being drawn from same parent distribution of $p = 0.56$. Further stacking analysis of the 80 FIR undetected quasars in our sample also finds no statistically significant difference in the SFR distribution for both the quasars with Mg II AALs and without Mg II AALs (see Section 2.3). These suggest that the quasars with Mg II AALs have indistinguishable FIR-based SFR distribution from those without Mg II AALs.

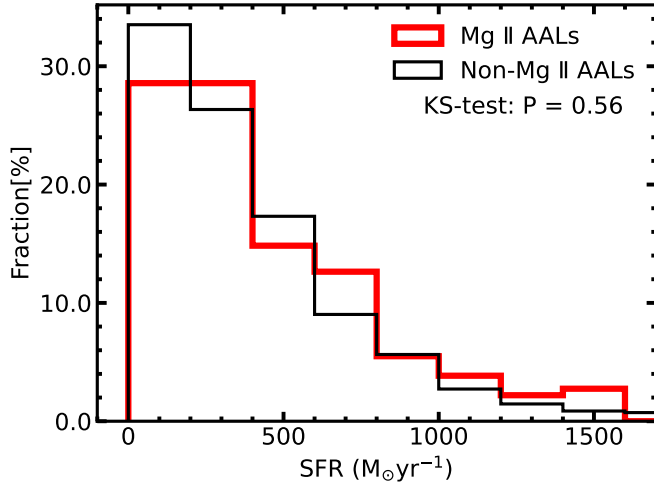


Figure 3: The SFR distributions for quasars with (red line) and without (black line) Mg II AALs. Here the IR emissions from AGN dust are based on the template from Lani et al. (2017).

The AGN contributions to the FIR emission are different for different AGN templates, which may lead to a discrepancy in estimates of the SFRs of AGN host galaxies. Different from the AGN template from Lani et al. (2017), the AGN template from Symeonidis et al. (2016, 2022) has non-negligible contributions to the FIR emission, and powerful AGN tends to have a greater contribution. To assess the effect of AGN template on the SFR distributions of the two types of quasars, we repeat the work as done in 2.2 by replacing with the template of Symeonidis et al. (2016, 2022). Then the results are shown in Figure 4. One could find from the figure that, a large p-value ($p = 0.60$) indicates the two types of quasars almost share the same SFR distributions, with the median SFRs are 318^{+487}_{-203} and 305^{+452}_{-209} $M_{\odot} \text{ yr}^{-1}$ for the quasars with and without Mg II AALs, respectively, which are systematically slightly smaller than those derived from the AGN template of Lani et al. (2017). This should be the cause that the AGN template of Symeonidis et al. (2016, 2022) contributes systematically more to FIR emissions than that of Lani et al. (2017).

Interestingly, What accounts for the observed distribution in Figures of 3 and 4? Although it is believed that the SFR density is redshift-dependent, with a peak at approximately 3.5 Gyr ($z \sim 2$) after the Big Bang (Madau & Dickinson 2014), we believe that the quasar redshifts in our sample play a less role in producing similar SFR distributions based on the following evidences: firstly, as shown in Figure 1, the null hypothesis probability ($p = 0.25$) returned by a 1-D KS-test indicates that one can not reject the two types of quasars come

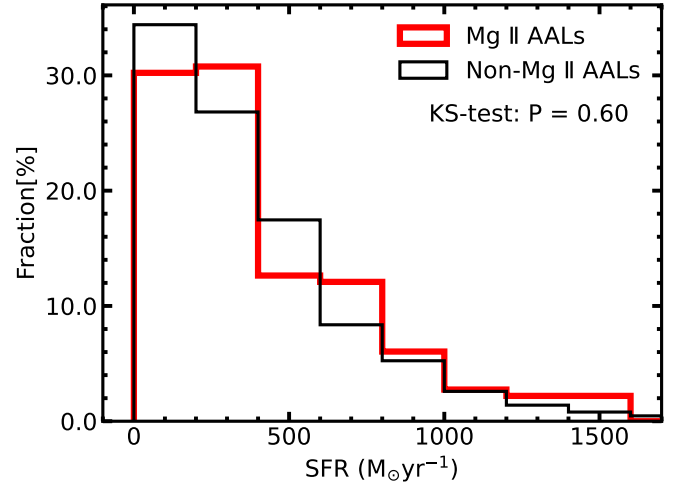


Figure 4: The same as Figure 3 but based on the template from Symeonidis et al. (2022).

from the same parent distribution. Next, shown in Figure 5 are the relationships between the SFRs of the two types of quasars derived from the AGN template of Lani et al. (2017) and their corresponding redshifts. Again, the null hypothesis probability ($p = 0.11$) returned by a 2-D KS-test (Peacock 1983) on the SFR-redshift distributions indicates no statistically significant difference between them.

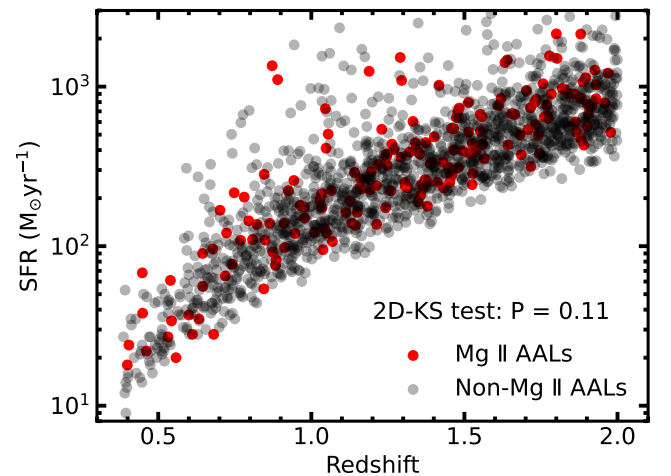


Figure 5: The z-SFR distributions for the quasars with (red points) and without (gray points) Mg II AAL. The 2D-KS test yields a probability $p = 0.11$.

The SFR is also related to its stellar mass within the host galaxy. Although the stellar masses of our sample's quasars host galaxies are not available from the current literature, we could use the virial black hole masses pro-

vided by Wu & Shen (2022) and Huang et al. (2023) as a proxy of the stellar masses due to a tight correlation between the two quantities (Kormendy & Ho 2013). Finally we identify that the median black hole masses of the quasars with and without Mg II AALs are $10^{8.79^{+0.65}_{-0.48}} M_{\odot}$ and $10^{8.70^{+0.50}_{-0.52}} M_{\odot}$, respectively. This also suggests that the stellar masses within host galaxies in our sample play a less role in producing the two indistinguishable FIR-based SFR distributions as shown in Figures of 3 and 4.

In the evolution scheme, the quasars with Mg II AALs are expected to host redder spectra and higher SFRs relative to those without Mg II AALs (e.g., Shen & Ménard 2012; Chen et al. 2022; Peng et al. 2024). In the orientation-dependent scheme, the quasars with Mg II AALs would also exhibit redder spectra relative to those without Mg II AALs, but both types of quasars are expected to have similar SFRs. As shown in Figure 6, our analysis clearly shows that the quasars with Mg II AALs obviously exhibit redder median composite spectra compared to those without Mg II AALs. However, quasars with Mg II AALs are statistically indistinguishable in terms of the SFR distribution from those without Mg II AALs (see Figure 3 or 4). The observations are not supported by the evolutionary model, which puzzle us. Similar observed signatures have also been found between the HiBAL and Non-BAL quasars (Cao Orjales et al. 2012), in which a simple orientation scheme was invoked to interpret. At the same time, some authors (Richards et al. 2001; Vestergaard 2003; Stone & Richards 2019) have also suggested that some AALs are the result of an outflow from the accretion disc, perhaps in a direction at some angle to our line of sight. Being reminded of this, we speculate that the orientation effect may be a possible channel for reconciling the observations seen in Figure 6. We will further investigate the properties of the AALs when the angles of quasar’s sightlines can be limited with more available data, so that ones can comprehend more deeply the influences of the evolution and orientation effects on the formation of the quasar’s AALs.

We also notice that some of the SPIRE fluxes may be contaminated with non-thermal emission, especially

for radio-detected quasars. There are only 120 radio-detected quasars in our sample. Thus we exclude these sources from our sample and still find no statistically significant difference in the SFR distribution for both the quasars with Mg II AALs and without Mg II AALs, indicating that the contamination, if any, do not bias our conclusions. But a caution is warranted regarding our findings in view of the following facts: The full width half maximum (FWHM) of SPIRE point spread functions (PSF) (beam size) are larger than $18''$, reaching $36''$ at $500 \mu\text{m}$ (see SPIRE Handbook²). These low resolutions lead to a chance that sources physically associated with the quasars, or just the chance line of sight sources, which would contaminate the flux of quasar of interest to us, and now we can not eliminate this contamination with available data. This may bias our findings.

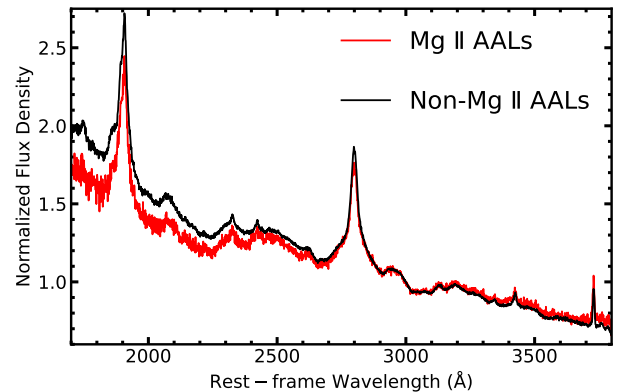


Figure 6: The median composite spectra of the Non-Mg II AAL (black line) and Mg II AAL (red line) quasars.

ACKNOWLEDGEMENTS

This work is supported by This work is supported by the Guangxi Natural Science Foundation (2024GXNSF262DA010069), the National Natural Science Foundation of China (grant No. 12133003, 12473011), and the Scientific Research Project of Guangxi University for Nationalities (2018KJQD01). We deeply thank the anonymous referees for her/his helpful and careful comments.

REFERENCES

- Abazajian, K. N., Adelman-McCarthy, J. K., Agüeros, M. A., et al. 2009, *ApJS*, 182, 543, doi: 10.1088/0067-0049/182/2/543

² http://herschel.esac.esa.int/Docs/SPIRE/spire_handbook.pdf

- Allen, J. T., Hewett, P. C., Maddox, N., Richards, G. T., & Belokurov, V. 2011, *MNRAS*, 410, 860, doi: [10.1111/j.1365-2966.2010.17489.x](https://doi.org/10.1111/j.1365-2966.2010.17489.x)
- Antonucci, R. 1993, *ARA&A*, 31, 473, doi: [10.1146/annurev.aa.31.090193.002353](https://doi.org/10.1146/annurev.aa.31.090193.002353)
- Assef, R. J., Stern, D., Noirot, G., et al. 2018, *ApJS*, 234, 23, doi: [10.3847/1538-4365/aaa00a](https://doi.org/10.3847/1538-4365/aaa00a)
- Bianchini, F., Fabbian, G., Lapi, A., et al. 2019, *ApJ*, 871, 136, doi: [10.3847/1538-4357/aaf86b](https://doi.org/10.3847/1538-4357/aaf86b)
- Bieri, R., Dubois, Y., Silk, J., Mamon, G. A., & Gaibler, V. 2016, *MNRAS*, 455, 4166, doi: [10.1093/mnras/stv2551](https://doi.org/10.1093/mnras/stv2551)
- Boroson, T. A. 1992, *The Astrophysical Journal Letters*, 399, L15, doi: [10.1086/186595](https://doi.org/10.1086/186595)
- Bouché, N., Finley, H., Schroetter, I., et al. 2016, *ApJ*, 820, 121, doi: [10.3847/0004-637X/820/2/121](https://doi.org/10.3847/0004-637X/820/2/121)
- Calzetti, D., Armus, L., Bohlin, R. C., et al. 2000, *ApJ*, 533, 682, doi: [10.1086/308692](https://doi.org/10.1086/308692)
- Cao Orjales, J. M., Stevens, J. A., Jarvis, M. J., et al. 2012, *MNRAS*, 427, 1209, doi: [10.1111/j.1365-2966.2012.22049.x](https://doi.org/10.1111/j.1365-2966.2012.22049.x)
- Casey, C. M. 2012, *MNRAS*, 425, 3094, doi: [10.1111/j.1365-2966.2012.21455.x](https://doi.org/10.1111/j.1365-2966.2012.21455.x)
- Chen, Z., He, Z., Ho, L. C., et al. 2022, *Nature Astronomy*, 6, 339, doi: [10.1038/s41550-021-01561-3](https://doi.org/10.1038/s41550-021-01561-3)
- Chen, Z.-F., Gu, Q.-S., Zhou, L., & Chen, Y.-M. 2016, *MNRAS*, 462, 2980, doi: [10.1093/mnras/stw1872](https://doi.org/10.1093/mnras/stw1872)
- Chen, Z.-F., Huang, W.-R., Pang, T.-T., et al. 2018, *ApJS*, 235, 11, doi: [10.3847/1538-4365/aaaaec](https://doi.org/10.3847/1538-4365/aaaaec)
- Chen, Z.-F., Qin, H.-C., Chen, Z.-G., et al. 2020, *ApJ*, 893, 25, doi: [10.3847/1538-4357/ab7896](https://doi.org/10.3847/1538-4357/ab7896)
- Ciesla, L., Charmandaris, V., Georgakakis, A., et al. 2015, *A&A*, 576, A10, doi: [10.1051/0004-6361/201425252](https://doi.org/10.1051/0004-6361/201425252)
- Crichton, D., Gralla, M. B., Hall, K., et al. 2016, *MNRAS*, 458, 1478, doi: [10.1093/mnras/stw344](https://doi.org/10.1093/mnras/stw344)
- Dawson, K. S., Schlegel, D. J., Ahn, C. P., et al. 2013, *AJ*, 145, 10, doi: [10.1088/0004-6256/145/1/10](https://doi.org/10.1088/0004-6256/145/1/10)
- Draine, B. T. 2006, *ApJ*, 636, 1114, doi: [10.1086/498130](https://doi.org/10.1086/498130)
- Fabian, A. C. 2012, *ARA&A*, 50, 455, doi: [10.1146/annurev-astro-081811-125521](https://doi.org/10.1146/annurev-astro-081811-125521)
- Foreman-Mackey, D., Hogg, D. W., Lang, D., & Goodman, J. 2013, *PASP*, 125, 306, doi: [10.1086/670067](https://doi.org/10.1086/670067)
- Gaibler, V., Khochfar, S., Krause, M., & Silk, J. 2012, *MNRAS*, 425, 438, doi: [10.1111/j.1365-2966.2012.21479.x](https://doi.org/10.1111/j.1365-2966.2012.21479.x)
- Galliano, F., Dwek, E., & Chantal, P. 2008, *ApJ*, 672, 214, doi: [10.1086/523621](https://doi.org/10.1086/523621)
- Gibson, R. R., Jiang, L., Brandt, W. N., et al. 2009, *ApJ*, 692, 758, doi: [10.1088/0004-637X/692/1/758](https://doi.org/10.1088/0004-637X/692/1/758)
- Hamann, F., Simon, L., Rodriguez Hidalgo, P., & Capellupo, D. 2012, in *Astronomical Society of the Pacific Conference Series*, Vol. 460, *AGN Winds in Charleston*, ed. G. Chartas, F. Hamann, & K. M. Leighly, 47. <https://arxiv.org/abs/1204.3791>
- Hopkins, P. F., Hernquist, L., Cox, T. J., & Kereš, D. 2008, *ApJS*, 175, 356, doi: [10.1086/524362](https://doi.org/10.1086/524362)
- Hopkins, P. F., Torrey, P., Faucher-Giguère, C.-A., Quataert, E., & Murray, N. 2016, *MNRAS*, 458, 816, doi: [10.1093/mnras/stw289](https://doi.org/10.1093/mnras/stw289)
- Huang, W.-R., Chen, Z.-G., Chen, Z.-F., & Li, X.-F. 2023, *ApJS*, 264, 52, doi: [10.3847/1538-4365/aca6e2](https://doi.org/10.3847/1538-4365/aca6e2)
- Kennicutt, Jr., R. C. 1998, *ARA&A*, 36, 189, doi: [10.1146/annurev.astro.36.1.189](https://doi.org/10.1146/annurev.astro.36.1.189)
- Khostovan, A. A., Malhotra, S., Rhoads, J. E., et al. 2020, *MNRAS*, 493, 3966, doi: [10.1093/mnras/staa175](https://doi.org/10.1093/mnras/staa175)
- Kormendy, J., & Ho, L. C. 2013, *ARA&A*, 51, 511, doi: [10.1146/annurev-astro-082708-101811](https://doi.org/10.1146/annurev-astro-082708-101811)
- Lani, C., Netzer, H., & Lutz, D. 2017, *MNRAS*, 471, 59, doi: [10.1093/mnras/stx1374](https://doi.org/10.1093/mnras/stx1374)
- Lyke, B. W., Higley, A. N., McLane, J. N., et al. 2020, *ApJS*, 250, 8, doi: [10.3847/1538-4365/aba623](https://doi.org/10.3847/1538-4365/aba623)
- Madau, P., & Dickinson, M. 2014, *ARA&A*, 52, 415, doi: [10.1146/annurev-astro-081811-125615](https://doi.org/10.1146/annurev-astro-081811-125615)
- Mor, R., & Netzer, H. 2012, *MNRAS*, 420, 526, doi: [10.1111/j.1365-2966.2011.20060.x](https://doi.org/10.1111/j.1365-2966.2011.20060.x)
- Netzer, H., Lani, C., Nordon, R., et al. 2016, *ApJ*, 819, 123, doi: [10.3847/0004-637X/819/2/123](https://doi.org/10.3847/0004-637X/819/2/123)
- Nguyen, H. T., Schulz, B., Levenson, L., et al. 2010, *A&A*, 518, L5, doi: [10.1051/0004-6361/201014680](https://doi.org/10.1051/0004-6361/201014680)
- NHSC. 2020a, *Herschel SPIRE Point Source Catalog: 250 microns*, NASA IPAC DataSet, IRSA45, doi: [10.26131/IRSA45](https://doi.org/10.26131/IRSA45)
- . 2020b, *Herschel SPIRE Point Source Catalog: 350 microns*, NASA IPAC DataSet, IRSA46, doi: [10.26131/IRSA46](https://doi.org/10.26131/IRSA46)
- . 2020c, *Herschel SPIRE Point Source Catalog: 500 microns*, NASA IPAC DataSet, IRSA44, doi: [10.26131/IRSA44](https://doi.org/10.26131/IRSA44)
- Peacock, J. A. 1983, *MNRAS*, 202, 615, doi: [10.1093/mnras/202.3.615](https://doi.org/10.1093/mnras/202.3.615)
- Peng, X.-L., Chen, Z.-F., He, Z.-C., Pang, T.-T., & Wang, Z.-W. 2024, *ApJ*, 963, 3, doi: [10.3847/1538-4357/ad1e5e](https://doi.org/10.3847/1538-4357/ad1e5e)
- Pitchford, L. K., Hatziminaoglou, E., Feltre, A., et al. 2016, *MNRAS*, 462, 4067, doi: [10.1093/mnras/stw1840](https://doi.org/10.1093/mnras/stw1840)
- Priddey, R. S., & McMahan, R. G. 2001, *MNRAS*, 324, L17, doi: [10.1046/j.1365-8711.2001.04548.x](https://doi.org/10.1046/j.1365-8711.2001.04548.x)
- Richards, G. T., Laurent-Muehleisen, S. A., Becker, R. H., & York, D. G. 2001, *ApJ*, 547, 635, doi: [10.1086/318414](https://doi.org/10.1086/318414)

- Sanders, D. B., Soifer, B. T., Elias, J. H., et al. 1988, *ApJ*, 325, 74, doi: [10.1086/165983](https://doi.org/10.1086/165983)
- Shen, Y., & Ménard, B. 2012, *ApJ*, 748, 131, doi: [10.1088/0004-637X/748/2/131](https://doi.org/10.1088/0004-637X/748/2/131)
- Smee, S. A., Gunn, J. E., Uomoto, A., et al. 2013, *AJ*, 146, 32, doi: [10.1088/0004-6256/146/2/32](https://doi.org/10.1088/0004-6256/146/2/32)
- Stanley, F., Alexander, D. M., Harrison, C. M., et al. 2017, *MNRAS*, 472, 2221, doi: [10.1093/mnras/stx2121](https://doi.org/10.1093/mnras/stx2121)
- Stone, R. B., & Richards, G. T. 2019, *MNRAS*, 488, 5916, doi: [10.1093/mnras/stz2111](https://doi.org/10.1093/mnras/stz2111)
- Symeonidis, M., Giblin, B. M., Page, M. J., et al. 2016, *MNRAS*, 459, 257, doi: [10.1093/mnras/stw667](https://doi.org/10.1093/mnras/stw667)
- Symeonidis, M., Maddox, N., Jarvis, M. J., et al. 2022, *MNRAS*, 514, 4450, doi: [10.1093/mnras/stac1359](https://doi.org/10.1093/mnras/stac1359)
- Urry, C. M., & Padovani, P. 1995, *PASP*, 107, 803, doi: [10.1086/133630](https://doi.org/10.1086/133630)
- Valiante, E., Smith, M. W. L., Eales, S., et al. 2016, *MNRAS*, 462, 3146, doi: [10.1093/mnras/stw1806](https://doi.org/10.1093/mnras/stw1806)
- Vestergaard, M. 2003, *ApJ*, 599, 116, doi: [10.1086/379159](https://doi.org/10.1086/379159)
- Viero, M. P., Asboth, V., Roseboom, I. G., et al. 2014, *ApJS*, 210, 22, doi: [10.1088/0067-0049/210/2/22](https://doi.org/10.1088/0067-0049/210/2/22)
- Wang, T., Ferland, G. J., Yang, C., Wang, H., & Zhang, S. 2016, *The Astrophysical Journal*, 824, 106, doi: [10.3847/0004-637X/824/2/106](https://doi.org/10.3847/0004-637X/824/2/106)
- Wethers, C. F., Kotilainen, J., Schramm, M., & Schulze, A. 2020, *MNRAS*, 498, 1469, doi: [10.1093/mnras/staa2017](https://doi.org/10.1093/mnras/staa2017)
- Willott, C., Rawlings, S., & Grimes, J. 2004, in *Astronomical Society of the Pacific Conference Series*, Vol. 311, *AGN Physics with the Sloan Digital Sky Survey*, ed. G. T. Richards & P. B. Hall, 223, doi: [10.48550/arXiv.astro-ph/0310653](https://doi.org/10.48550/arXiv.astro-ph/0310653)
- Wu, Q., & Shen, Y. 2022, *ApJS*, 263, 42, doi: [10.3847/1538-4365/ac9ead](https://doi.org/10.3847/1538-4365/ac9ead)
- York, D. G., Adelman, J., Anderson, Jr., J. E., et al. 2000, *AJ*, 120, 1579, doi: [10.1086/301513](https://doi.org/10.1086/301513)
- Zhuang, M.-Y., & Ho, L. C. 2019, *ApJ*, 882, 89, doi: [10.3847/1538-4357/ab340d](https://doi.org/10.3847/1538-4357/ab340d)